JOURNAL OF GEOPHYSICAL RESEARCH, VOL. 114, B00A15, doi:10.1029/2008JB006062, 2009

Complex nonvolcanic tremor near Parkfield, California, triggered by the great 2004 Sumatra earthquake

Abhijit Ghosh,[1] John E. Vidale,[1] Zhigang Peng,[2] Kenneth C. Creager,[1] and Heidi Houston[1]

Received 1 September 2008; revised 29 January 2009; accepted 21 August 2009; published 4 December 2009.

[1] In several instances, the passing surface waves from large earthquakes have ignited nonvolcanic tremor (NVT) on major faults. Still, the mechanism of tremor and its reaction to the dynamic stressing from various body and surface waves is poorly understood. We examine tremor near Parkfield, California, beneath the San Andreas fault triggered by the Mw 9.2, 2004 Sumatra earthquake. The prolonged shaking produces the richest and the most varied observations of dynamically triggered tremor to date. The tremor appears in at least three distinct locations and shows activity pulsing with encouraging stress, as has been observed in other cases. The greatest amount of triggering and tremor modulation accompanies the long-period Love waves. Rayleigh waves, on the other hand, appear to be less effective in exciting tremor sources. Also, at times, the tremor stops before the surface waves are complete, at other times it continues quivering after the waves have passed. While tremor is found to be sensitive to small stress changes, there are times when stresses of comparable magnitudes do not trigger noticeable tremor. Some tremors in this NVT sequence appear to be associated with the passage of *P* waves, which is unusual and surprising given the small stresses they impart.

Citation: Ghosh, A., J. E. Vidale, Z. Peng, K. C. Creager, and H. Houston (2009), Complex nonvolcanic tremor near Parkfield, California, triggered by the great 2004 Sumatra earthquake, *J. Geophys. Res.*, *114*, B00A15, doi:10.1029/2008JB006062.

1. Introduction

[2] Nonvolcanic tremor (NVT) is characterized by apparently noise-like, emergent waveforms that are depleted in high-frequency energy compared to ordinary small earthquakes; lasts for a few seconds to days; and has envelopes that are coherent across many seismic stations miles apart. It was first found in the subduction zone of southwest Japan [*Obara*, 2002], and subsequent studies have revealed tremor activities in other subduction zones including Cascadia [*Rogers and Dragert*, 2003], Mexico [*Payero et al.*, 2008], Costa Rica [*Thorwart et al.*, 2007], and Alaska [*Peterson and Christensen*, 2009]. Strong tremor activity is often associated with prominent geodetic signals indicating slow slip at the subduction interface. Episodic tremor and slip (ETS) is the term coined by *Rogers and Dragert* [2003] to describe this remarkably periodic coupled phenomenon in the Cascadia subduction zone. Recent studies find tremor activity along the San Andreas fault (SAF), a continental transform plate boundary fault [*Ellsworth et al.*, 2005; *Nadeau and Dolenc*, 2005; *Shelly et al.*, 2009], and beneath the central Range in Taiwan, an arc-continental type collision environment [*Peng and Chao*, 2008], showing that NVT is not limited to subduction environments. The tremor mechanism, however, remains elusive. Some subduction zone tremor studies suggest that fluids released due to dehydration reactions in the slab cause NVT [e.g., *Kao et al.*, 2005; *Obara*, 2002], while other works indicate that tremor may be caused by many small shear failures, i.e., low-frequency earthquakes (LFE), occurring in a very short time interval [e.g., *Ide et al.*, 2007; *Shelly et al.*, 2006, 2007a]. Using a dense seismic array in Cascadia, A. Ghosh et al. (Tremor streaks in Cascadia, manuscript in preparation, 2009) find streaks of tremor that propagate rapidly and argue that a combination of fluid flow and shear slip is responsible for such rapid and continuous tremor migration over short time scale. In addition, much of the seismic tremor moment during a slow slip event is released by several distinct patches, which may indicate wet spots on the interface [*Ghosh et al.*, 2009].

[3] NVT is sensitive to very small stress perturbations and even modulated by tiny tidal stressing [*Shelly et al.*, 2007b; *Rubinstein et al.*, 2008; *Nakata et al.*, 2008; *Nadeau et al.*, 2008]. Small changes in static stress induced by NVT activity itself are able to stimulate tremor activity in the nearby area on the fault (A. Ghosh et al., Tremor bands sweep Cascadia, submitted manuscript, 2009). On the other hand, dynamic stresses generated by large teleseismic events have triggered tremor in several instances. In the Nankai subduction zone in southwestern Japan, the 2004 Mw 9.2 Sumatra earthquake triggered NVT that correlates with the passing Rayleigh waves [*Miyazawa and Brodsky*, 2008; *Miyazawa and Mori*, 2006]. They argue that dilatational stress produced by the Rayleigh waves is responsible

[1]Department of Earth and Space Sciences, University of Washington, Seattle, Washington, USA.
[2]School of Earth and Atmospheric Sciences, Georgia Institute of Technology, Atlanta, Georgia, USA.

0148-0227/09/2008JB006062$09.00

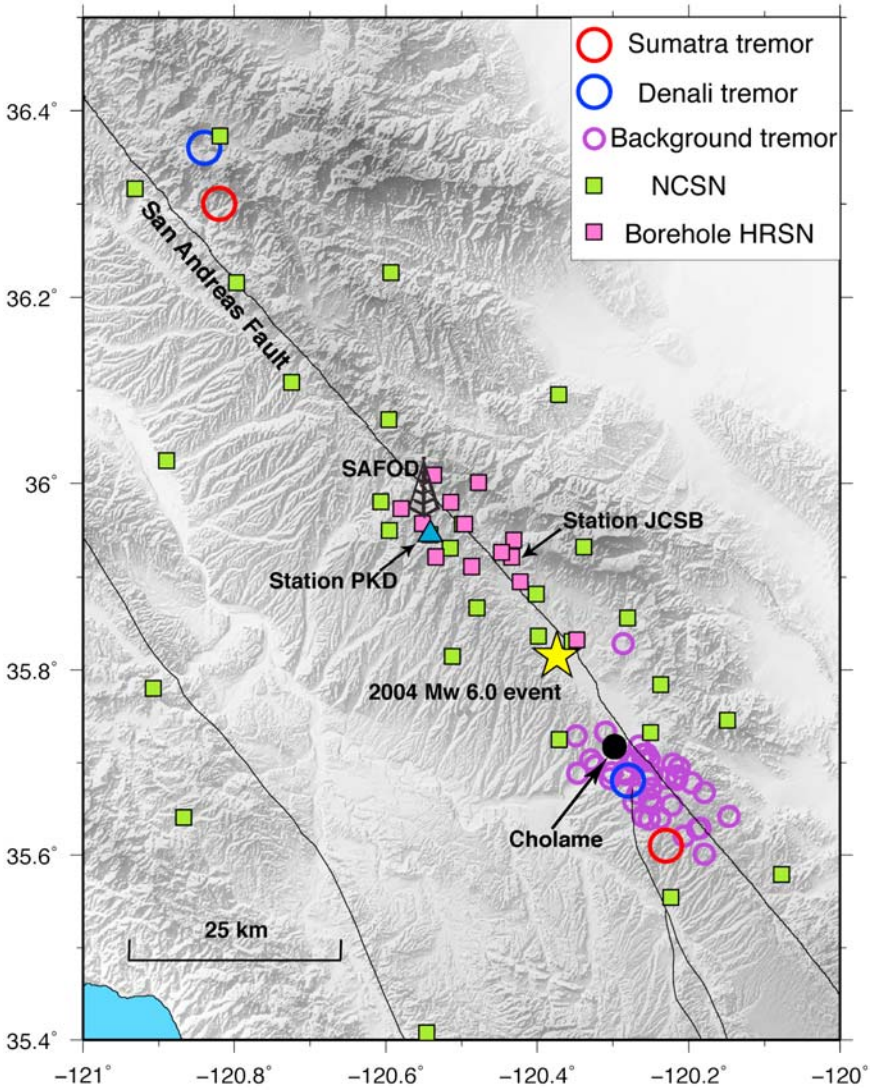

Figure 1. A map of the study area around the Parkfield section of the SAF. Gray lines denote surface traces of faults. Seismic stations of several networks are denoted with different symbols. The wellhead of San Andreas Fault Observatory at Depth (SAFOD), Cholame, borehole station JCSB of HRSN, and the broadband station PKD are labeled. The epicenter of the 2004 Mw 6.0 Parkfield earthquake, background tremor, source regions of NVT triggered by the 2004 Mw 9.2 Sumatra event, and 2002 Mw 7.8 Denali fault event are marked with different symbols and colors.

for triggering NVT, and infer that fluids play an important role in tremor mechanism. On the other hand, the Mw 7.8 Denali fault earthquake in 2002 sparked abundant NVT at Vancouver Island in the Cascadia subduction zone [*Rubinstein et al.*, 2007], and SAF [*Gomberg et al.*, 2008; *Peng et al.*, 2008, 2009] as well. Recently, *Peng and Chao* [2008] found clear NVT beneath the central Range in Taiwan triggered by the 2001 Mw 7.8 Kunlun earthquake. In all these cases, passing Love wave cycles correspond to the strongest tremor bursts, indicating transient shear stress as the driving mechanism of triggered NVT. Hence, the way different stressing conditions influence the generation of NVT is still an important unresolved issue.

[4] Here, we study the response of NVT near Parkfield along the SAF during the great Mw 9.2 Sumatra earthquake in 2004 [*Lay et al.*, 2005]. We choose this event because of its enormous size, and the strong shaking it caused around the world. Indeed, previous studies have shown that this event triggered microearthquakes in Alaska [*West et al.*, 2005], NVT in Japan [*Miyazawa and Brodsky*, 2008; *Miyazawa and Mori*, 2006] and Cascadia [*Rubinstein et al.*, 2009], and possibly temporal changes in fault zone properties around the Parkfield section of the SAF [*Taira et al.*, 2009].

[5] Parkfield is a particularly apt place to study tremor, as it is one of the few nonsubduction zone environments where NVT has so far been identified [e.g., *Nadeau and Dolenc*, 2005]. Also, this area has very dense station coverage, including the sensitive borehole High-Resolution Seismic Network (HRSN) operated by the University of California, Berkeley, and the Northern California Seismic Network (NCSN) operated by the U.S. Geological Survey (Figure 1). The HRSN is a cluster of 13 borehole stations along the SAF with all the sites located within ~30 km of the epicenter of the 2004 Mw 6.0 Parkfield event [*Bakun et*

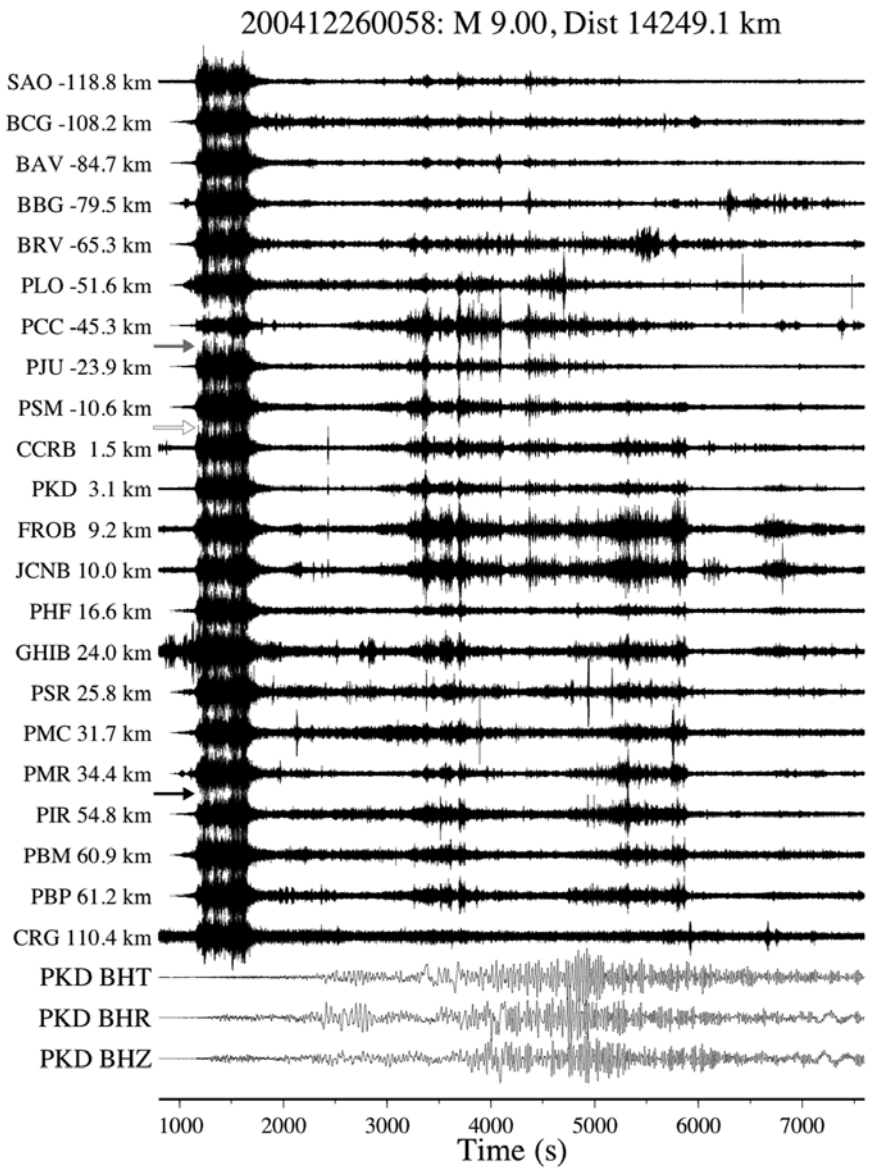

Figure 2. A record section of the 2–8 Hz band-pass-filtered vertical seismograms showing tremor during the passage of the teleseismic waves from 2004 Mw 9.2 Sumatra earthquake. The energy during *P* waves (~1000–2000 s) has contributions from both NVT and teleseismic body waves. Gray and black arrows indicate northern and southern sources of tremor, respectively, while the open arrow marks the location of the SAFOD site. Time is relative to the origin of the Sumatra event.

al., 2005]. It is equipped with three-component 2 Hz Mark Products L22, Geospace HS1, or Litton 1023 sensors, and records data at a rate of 20 and 250 samples per second. More details of the network are given by *Karageorgi et al.* [1992] and at http://seismo.berkeley.edu/bdsn/hrsn_overview.html. The NCSN, on the other hand, covers a larger area and is designed to detect local and regional earthquakes throughout central and northern California. It consists of 512 stations with a mixture of short-period, broadband, strong motion sensors, and some borehole sites. In this study, we analyze the tremor signals recorded by the short-period surface stations (1 Hz Mark Products L4C) in the NCSN and borehole HRSN. Figures S1 and S2 in the auxiliary material show the map of the stations used in this study.[1] We also analyzed the data recorded by the broadband station PKD, which contains a Streckeisen STS-2 Seismometer and is part of the Berkeley Digital Seismic Network.

[6] We observe a complex sequence of strong tremor activity near Parkfield along the SAF triggered by the Sumatra event (Figures 2 and 3). The time axes of Figures 2–8 are relative to the origin time of the Sumatra earthquake (26 December 2004, 0058:53.45 UTC, Advance National Seismic System catalog). Overall, we see four distinct tremor patterns. (1) During the later parts of the *PKP* wave, which is also the time of the compressional arrivals *PP* and *SKP*, there is relatively featureless tremor, (2) 100–200 s period Love waves generate two bursts of tremor, (3) stronger 20–50 s period Love and Rayleigh waves generate dozens of bursts of tremor, and (4) a final extended burst of tremor with a smooth envelope appears

[1] Auxiliary materials are available in the HTML. doi:10.1029/2008JB006062.

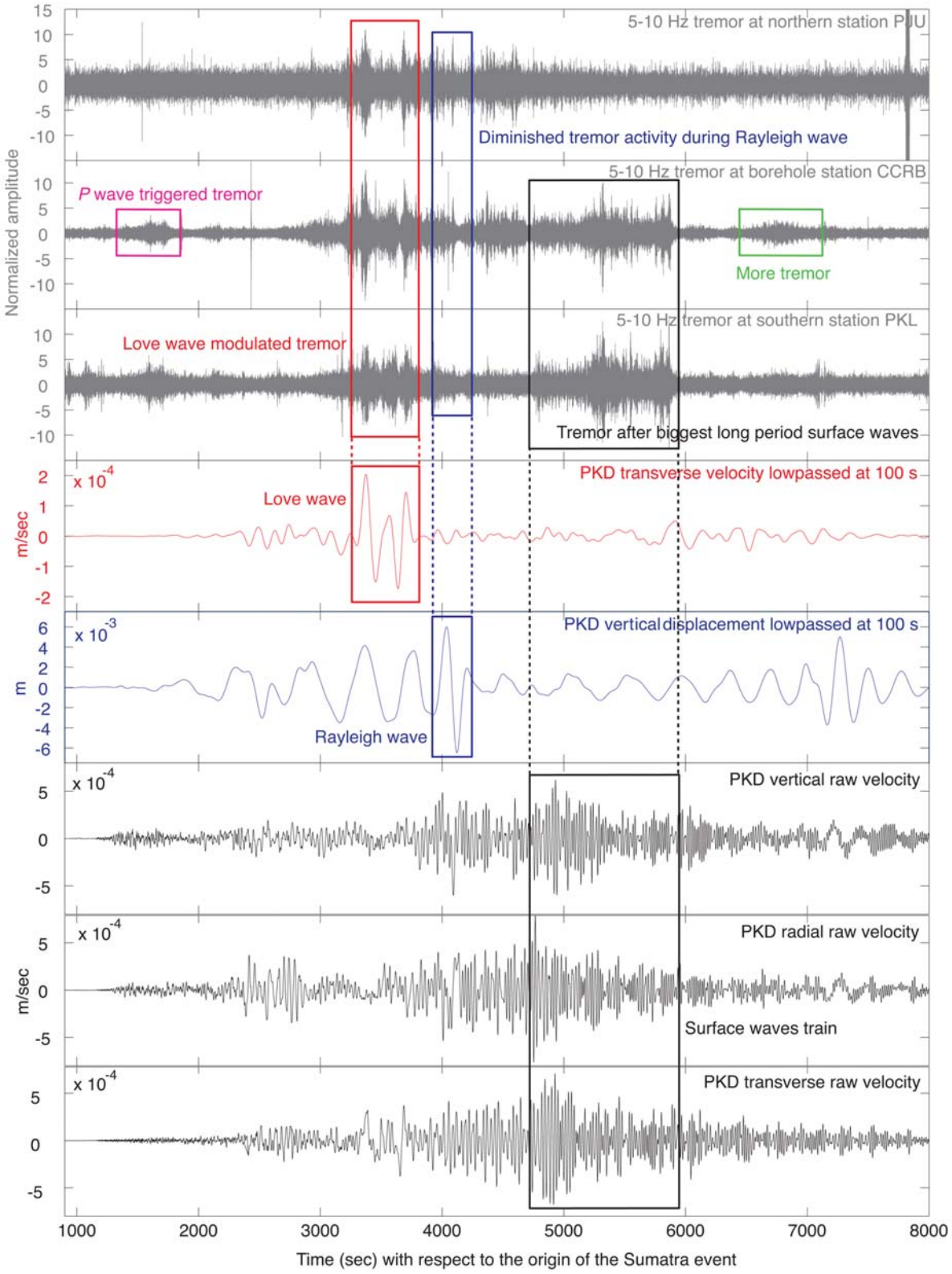

Figure 3. NVT during different teleseismic wave phases. Colored boxes highlight teleseismic waves in different time periods and corresponding tremors. First through third panels show 5–10 Hz tremor recorded at the northern, middle, and southern part of the study area. Fourth and fifth panels show long-period Love and Rayleigh waves ground motion, respectively, at station PKD. Sixth through eighth panels illustrate unfiltered velocity recorded at PKD. See annotations for details.

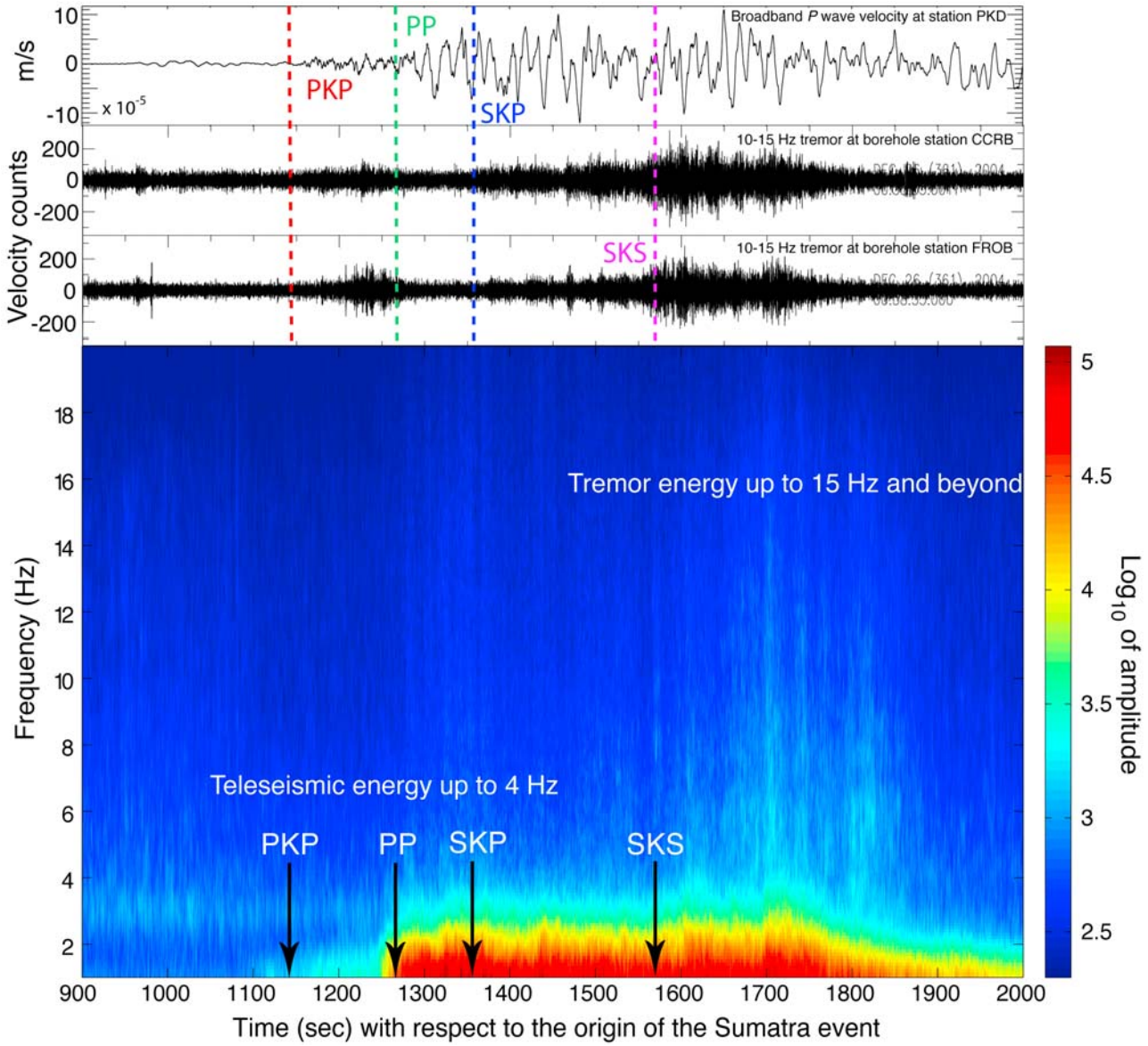

Figure 4. NVT during the passage of teleseismic body waves and the stacked spectrogram of 19 borehole HRSN channels with good signal-to-noise ratio. The seismograms show vertical component velocity at borehole HRSN stations CCRB and FROB, band-pass filtered at 10–15 Hz. The color dashed lines in the seismograms and black arrows in the spectrogram marked the theoretical first arrivals of the body wave phases from the Sumatra event. Theoretical teleseismic traveltimes are based on IASP91 Earth model [*Kennett and Engdahl*, 1991]. Note that the duration of the Sumatra earthquake is ~10 min. Notice tremor energy extends up to 15 Hz and beyond while most of the teleseismic body wave energy is restricted up to 4 Hz.

after most of the teleseismic shaking is over. Given the plethora of teleseismic action, the protracted Sumatra source duration, and the erratic nature of tremor, some of these associations are tentative. In the following sections, we examine the four tremor intervals, attempt to locate the tremor sources, compare the tremor activity to the driving stresses from the passing seismic waves, and explore the implications.

2. Triggering by *P* Waves

[7] Most triggering by teleseismic waves has so far been observed during the passage of the surface waves, which carry the greatest stress [*Hill*, 2008]. In this case, however, NVT starts during the arrivals of the *P* wave train traveling through the outer core (*PKP* group), which is also about the time of the *PP* and *SKP* arrivals (Figures 3, 4, and 5). As the Sumatra earthquake lasts for ~10 min [*Ishii et al.*, 2005], this tremor event, which lasts ~5 min, takes place when multiple body wave phases are coming in simultaneously. Stressing due to *SKS* is probably not an important factor in triggering this NVT event, because almost vertically incident *SKS* produces negligible strike-parallel shear stress on the vertical SAF, although *SKS* hits Parkfield around the time when tremor starts (Figure 4). It is difficult to locate

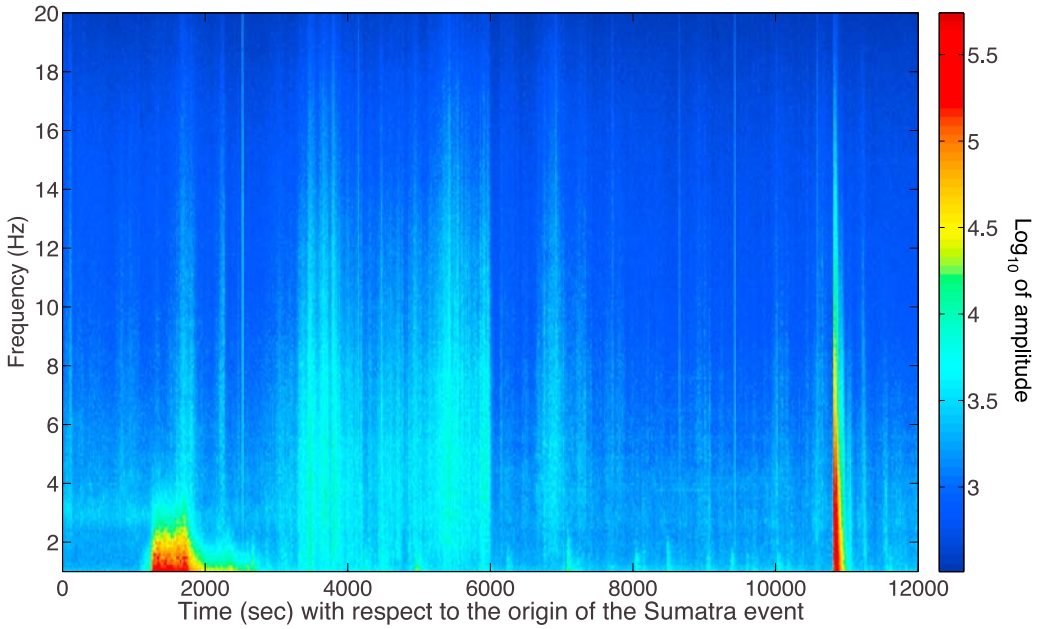

Figure 5. Stacked spectrogram of 19 borehole HRSN channels with high signal-to-noise ratio. Surface wave-triggered tremor energy is observed after ~3000 s. Tremor triggered by the body waves is seen at around 1700 s, when energy extends up to 15 Hz and beyond, similar to the tremor triggered by the surface waves. Note that energy up to 15 Hz and beyond can only be seen during tremors and local/regional earthquakes. The spike of strong energy at ~11000 s is an ordinary earthquake.

this *P* wave-triggered tremor precisely due to its featureless envelope. But it is much clearer on the borehole HRSN stations clustered around Parkfield than on more distant stations, in contrast to the later tremor, which are located tens of kilometers from Parkfield. Based on this observation, we infer that the *P* wave-triggered tremor most likely occurs near Parkfield.

[8] This is the first NVT event in this sequence of triggered tremor, and occurs long before the arrival of the surface waves. The spectrograms in Figures 4 and 5 show

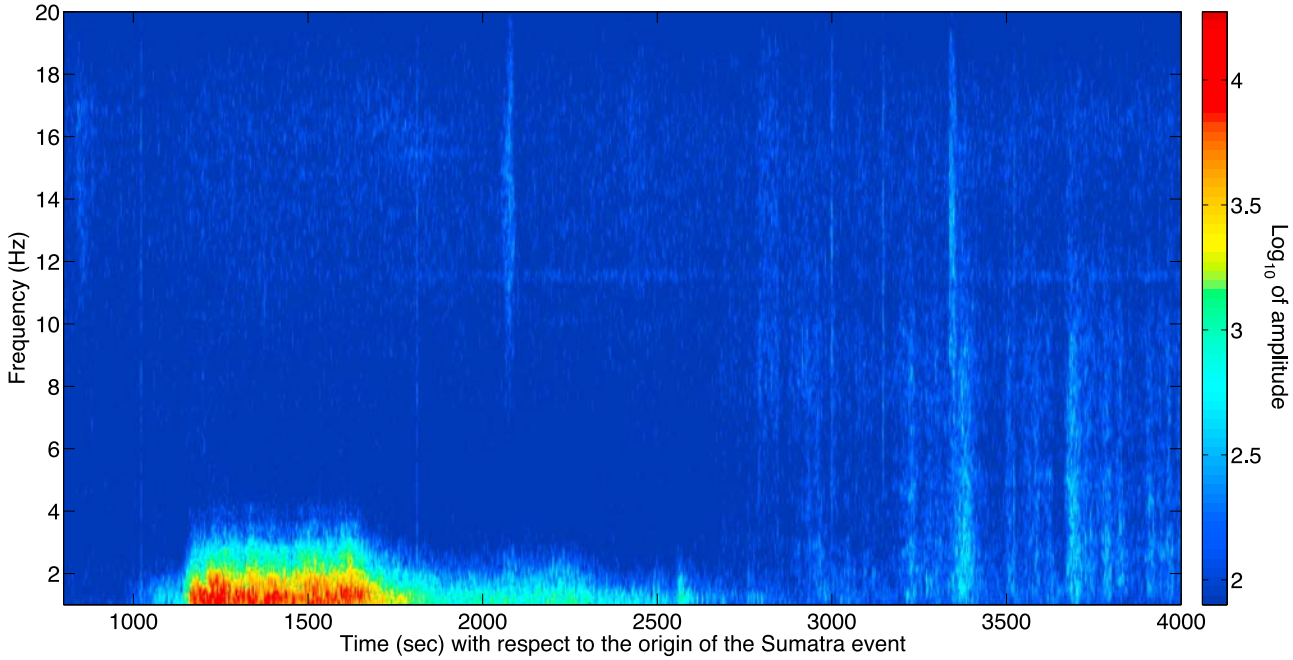

Figure 6. Stacked spectrogram of three NCSN vertical channels (station BJC, BMS, and PJU) situated tens of kilometers away from the inferred location of the tremor triggered by the teleseismic compressional waves. At this distance from the SAF, body wave energy goes only up to 4 Hz. Tremor energy up to 15 Hz and beyond is observed only after 3000 s during the passage of Love waves. Note absence of higher-frequency energy during the *P* wave-triggered tremor indicating its local origin.

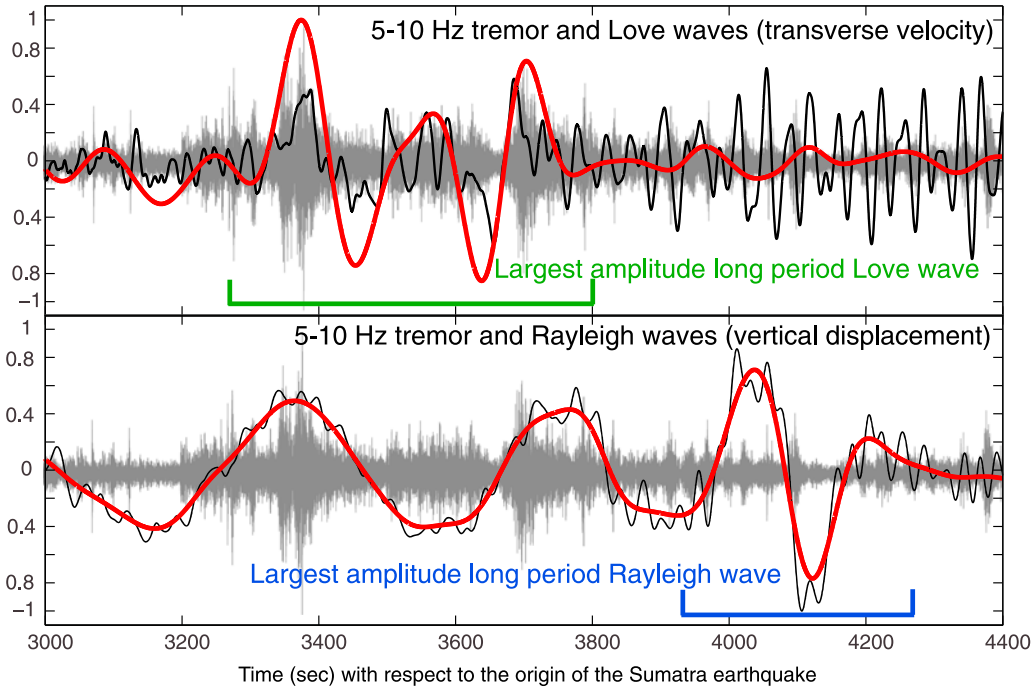

Figure 7. The 5–10 Hz tremor (gray), broadband surface waves (black), and surface waves low-pass filtered at 100 s (red) recorded at station PKD. Tremor is plotted after the time shift is applied (see text). (top) Transverse velocity (black and red). (bottom) Vertical displacement (black and red). Amplitudes are normalized, and no relative amplitude information is preserved. Long-period Love wave cycles matches almost perfectly with two strongest bursts of tremor. The largest-amplitude Rayleigh waves at ∼4100 s correspond to a time period of reduced NVT activity.

that the energy extends up to 15 Hz and beyond during this tremor event, similar to the frequency of much lucid tremor during the surface waves. This is in contrast to the earlier part of the PKP arrival, which shows strong body wave energy up to only 4 Hz. To check the possibility of the higher frequency energy near 15 Hz coming from the teleseismic body waves, we examine waveforms recorded by stations several tens of kilometers away from Parkfield, the inferred location of this tremor event. Analysis of these stations shows strong energy only up to 4 Hz during the passage of the teleseismic body waves, but almost none beyond that (Figure 6). It suggests that the higher frequency energy near 15 Hz observed near the HRSN is mostly of local origin (i.e., tremor), and not coming from the teleseismic body waves of the Sumatra event. In addition, automatic tremor detection algorithm also found tremor during this time period (R. Nadeau, personal communication, 2008), consistent with our observation.

[9] There are a few instances of tremor in the Parkfield region in the days prior the Sumatra earthquake. So it is conceivable that this initial burst of tremor during the *P* waves is coincidental. Perusals of a NVT catalog during the 20 days around 28 teleseismic events recorded near Parkfield region reveals that on average there are 0.3035 tremor events per day with duration of 5 min or longer (R. Nadeau, personal communication, 2008). However, no NVT events as strong as this one are seen the day just before the Sumatra earthquake. If we assume that the ambient tremor occurs randomly and each tremor event lasts around 5 min, the probability of having one tremor event in a 1000 s segment, which is the approximate duration of the passage of the strongest compressional body waves, would be 0.35%. Hence, a coincidence is unlikely.

[10] Near-vertical compressional waves apply minimal right-lateral shear stress to vertical faults, so the primary contribution of the *PKP* waves to the Coulomb stress on the SAF is via the fault-normal stress. Because most cases of teleseismically triggered tremor around Parkfield examined to date, including during the surface waves of this one, are dominated by Love wave triggering [*Peng et al.*, 2009], the *P* wave provides a good opportunity to compare the relative effectiveness of shear and normal stressing on the tremor generation.

[11] We assume that the tremor originated on the SAF near Parkfield for our stress analysis. This is plausible because the surface wave-triggered tremor sources in this region are near the trace of the SAF in map view, and previous studies have found tremor close to and consistent with slip on the SAF [*Nadeau and Dolenc*, 2005; *Shelly et al.*, 2009]. The depth of tremor in this area, estimated by other studies [*Nadeau and Dolenc*, 2005; *Shelly et al.*, 2009], is ∼25 km that we also assume here. For our stress calculation, we assume a vertically incident 20 s period *P* wave propagating in a Poisson solid. We choose this period because tests on a range of periods show that the largest stresses at station PKD during the Sumatra *P* wave train were around 20 s period. We consider the equation of the displacement for the 20 s harmonic waves, and calibrate it to the observed displacement at the station, factoring in the free-surface effect of increased amplitude of the displacement at the free surface. For this wave, we compute the strain tensor, and then determine the stress tensor using a

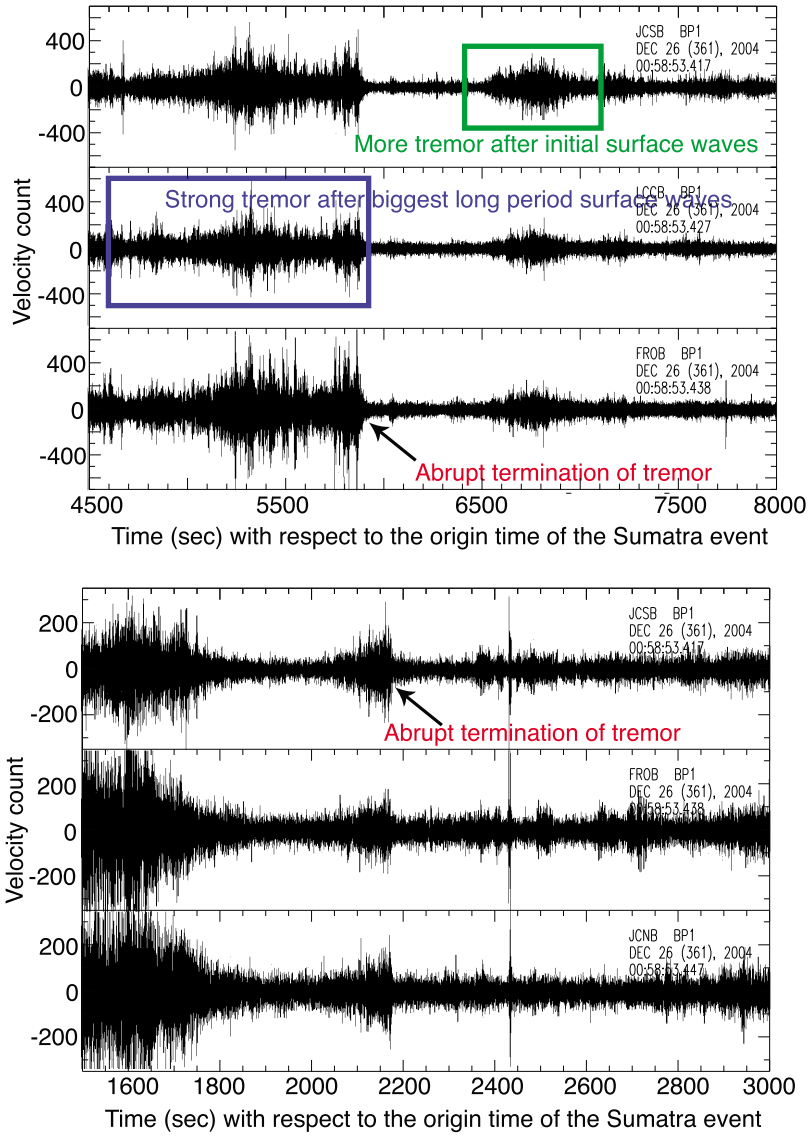

Figure 8. (top) Tremor excited near the end of the surface wave train at HRSN stations JCSB, LCCB, and FROB. Note abrupt ending of tremor at ~5900 s followed by reignited spindle-shaped tremor ~600 s later during relatively weak surface waves. (bottom) Another example of abrupt cessation of tremor at ~2200 s at HRSN stations JCSB, FROB, and JCNB. The spike at ~2430 s is a local earthquake.

shear modulus of 45.7 GPa, based on a 1-D velocity model of this area [*Oppenheimer et al.*, 1993].

[12] The estimated peak dilatational stress on the SAF at a depth of 25 km beneath station PKD is ~0.8 kPa. Such 20 s period *P* waves generate an even smaller (0.15 kPa) peak normal stress on the SAF. Because the dilatational stress is ~5 times larger than the normal stress, it is a more likely candidate to trigger the NVT event during the passage of the teleseismic *P* wave train, even though it is below the stress threshold for triggered NVT (2–3 kPa) inferred by *Peng et al.* [2009].

3. Triggering by Surface Waves

[13] We find that tremor is strongly modulated during the passage of the surface waves, with several vigorous tremor bursts synchronized with the Love wave cycles (Figures 3 and 7). Sharp fluctuations of the tremor amplitude, unlike the steadier tremor during the *P* wave, are indicative of the influence of stress modulation on tremor generation. To further quantify the relationship between the surface waves and tremor generation, we first use envelope cross correlation to locate tremor [*Wech and Creager*, 2008]. This is the same method used in our previous studies [*Rubinstein et al.*, 2007; *Gomberg et al.*, 2008; *Peng et al.*, 2008, 2009], and is similar to that used by *Obara* [2002]. After selecting a tremor time window (e.g., 3473–3819 s with respect to the origin of Sumatra event), we apply a band-pass filter from 3 to 8 Hz, calculate envelope functions, and low-pass filter those at 0.125 Hz. All pairs of envelope functions are cross-correlated. Tremor is located using a grid search method. For each location in the grid, the *S* wave traveltime difference for each station pair is computed, and the value of the cross correlation at that lag time is evaluated. Tremor

location is determined by maximizing the sum of weighted cross-correlation values using an L1 norm.

[14] NVT epicenters during the surface waves are located near the surface trace of the Parkfield segment of SAF, and concentrated in two regions (Figure 1). One region ($-120.22^\circ \pm 0.05^\circ$, $35.64^\circ \pm 0.05^\circ$) coincides with the background tremor locations around Cholame [*Nadeau and Dolenc*, 2005], near the transition between the locked and creeping part of the SAF. The other NVT source is about 100 km to the northwest ($-120.83^\circ \pm 0.10^\circ$, $36.33^\circ \pm 0.10^\circ$) in the creeping section of SAF near Bitterwater. Thus, this event excited NVT source regions nearby those triggered by the Mw 7.8 Denali fault earthquake in 2002 [*Gomberg et al.*, 2008; *Peng et al.*, 2008]. We do not torment the data further, for example seeking uncertainties and distinct locations for each pulse, due to the complicated teleseismic wave train and the complex tremor pattern. A better signal-to-noise ratio and simpler patterns allowed more detailed locations for the tremor from the Denali fault earthquake [*Rubinstein et al.*, 2007; *Peng et al.*, 2008].

[15] To analyze the relationship between the surface wave stressing and tremor pulses, we apply a time correction to both the surface waves and the tremor signal to account for the different arrival times for the surface waves between the recording station and the tremor source region, and the propagation of the tremor signals from the source region to the station. To do this, we first estimate the time differences of the surface wave arrivals between the station PKD and tremor source, using an average Love and Rayleigh wave phase velocities of 4.1 and 3.5 km/s respectively for this region [*Peng et al.*, 2008]. Then we use a 1-D velocity model for Parkfield [*Oppenheimer et al.*, 1993] to compute the *S* wave traveltime that determines the time for the tremor to arrive at PKD from its source. Combining these two time corrections, the final time shift is calculated. Figure 7 shows tremor and associated surface waves after the time correction is applied.

[16] For the stress calculation due to the surface waves, we remove the instrument response from the ground motion data recorded at PKD, and follow the method described by *Miyazawa and Brodsky* [2008]. The axes of the coordinate system are taken parallel to the radial (130.9° from north), transverse (220.9° from north), and vertical directions. The geometry is such that the propagation direction of the surface waves is almost parallel to the SAF strike of 139.2° from north [*Thurber et al.*, 2006]. The tremor is assumed to be located on the SAF, as in the case of *P* wave triggering. We begin with the solution for the Love wave equation [*Lay and Wallace*, 1995] in a slow velocity layer over a half-space. Physical properties of the layers are meant to model the Parkfield region. We use 4.0 and 4.2 km/s as the shear wave velocities of the top and bottom layer respectively, and 4.1 km/s as the phase velocity. The thickness of the top layer is taken to be 25 km. The layer velocities are kept close to each other so that the structure remains similar for the stress calculation for Rayleigh waves. Theoretical solutions for Love wave shear strain components at a depth of 25 km are normalized by the ground motion at the surface, and multiplied by observed ground motion at PKD to get the strain tensor 25 km beneath station PKD. We assume a Poisson solid, and from a 1-D velocity model for Parkfield area [*Oppenheimer et al.*, 1993], determine the shear modulus (45.7 GPa at 25 km depth) needed to calculate the stress tensor. Last, we rotated the coordinate system for the stress tensor such that the horizontal axes are parallel and perpendicular to the strike of the SAF.

[17] Previous studies have shown that for a vertical strike-slip fault, shear stress due to the Love waves most closely tracks the transverse velocity [*Hill*, 2008; *Peng et al.*, 2008], while dilatational stress due to Rayleigh wave is best represented by upward vertical surface displacement [*Miyazawa and Brodsky*, 2008; *Rubinstein et al.*, 2009]. Therefore, in Figures 3 and 7, we use the transverse velocity and vertical displacement as a proxy for stresses produced by Love and Rayleigh waves, respectively.

[18] The tremor rhythm generally matches well with the Love wave cycles (Figure 3 and 7), and the two biggest Love wave cycles coincide with the two strongest bursts of tremor energy. Long-period Love wave velocity, which has a favorable shear-stressing direction on the SAF, peaks at ~3380 s and ~3700 s, and matches closely with the tremor amplitude peaks during this time. The maximum shear stress on SAF at 25 km depth beneath the station PKD generated by the 160 s period Love wave from the Sumatra event is estimated to be ~3 kPa, which is significantly lower than the stresses calculated for the cases of 2002 Denali fault earthquake triggering NVT in Vancouver Island and Parkfield (~40 and ~20 kPa respectively) [*Rubinstein et al.*, 2007; *Peng et al.*, 2008].

[19] On the other hand, the largest Rayleigh wave pulse around 4100 s corresponds to a relatively quiet period of tremor activity (Figures 2, 3, and 7), despite generating much larger dilatational stress (~4 kPa for the dominant 30 s period Rayleigh wave) than during the *P* wave (~0.8 kPa). Peak dilatational stress produced by the Rayleigh wave is also higher than the Love wave-generated shear stress. For estimation of stress due to the Rayleigh wave, we use the solution for a simple half-space and apply a similar method as described above for the Love wave. Interestingly, the Rayleigh waves were shortly followed by a strong burst of tremor that continued for more than 15 min (Figures 2, 3, and 8). This tremor event coincides with the later phase of the surface wave train, and represents the longest tremor event in this entire triggered tremor sequence.

[20] There is also dilatational stress from the ~400 s period Rayleigh waves during the time period of peak amplitude Love waves, and associated bursts of tremor. The triggering potency of Love wave-induced shear stress vis-à-vis dilatational stress from Rayleigh waves in this time window is discussed in detail in section 5. Figure S3 shows tremor and teleseismic surface waves, all components, both velocity and displacement.

[21] The two NVT sources in the northern and southern parts of the area were triggered at different time periods during the passage of teleseismic waves. The only exception is observed during the passage of the large-amplitude long-period Love waves, when both sources simultaneously produced strong tremor. Right after the largest Love waves, and during the passage of the Rayleigh waves, the northern source was still pulsating while the southern source remained markedly silent (Figures 2 and 3). Tremor beating during this time matches better with the Love wave velocities rather than Rayleigh wave displacement. Immediately

after the biggest Rayleigh waves, the southern source became active and generated the longest NVT event of this tremor sequence, as mentioned above. In contrast, the northern source remained mostly calm during this time. These observations highlight the variability of the characteristics of different tremor sources. The stress necessary to arouse one tremor source may not be sufficient to excite another even though they are close together in space and time.

[22] The last clear tremor event in this sequence shows up at around 6500 s, after the passage of the initial surface waves, at a time with relatively weak surface waves, and lasted for ~8 min (Figures 3 and 8). This feeble but clear NVT event has a distinct spindle shape: it grows slowly in amplitude in the first half, and decays down at almost the same rate in the end with no abrupt amplitude fluctuations in between.

4. Tremor Reappearance and Abrupt Termination

[23] We observe intriguingly sudden cessations of NVT activity at least twice during this triggered tremor sequence. Just after the passage of the compressional wave train, a tremor event around 2100 s lasts only for ~2 min, then fades completely before the arrival of initial surface waves (Figure 8). A close scrutiny of the record from the borehole site JCSB (Figure 1) reveals that during most of its short lifetime, it grows in amplitude to ~15 times above the background activity, and dies with astonishing haste in the last 15 s (Figure 8). Neither the start nor the sharp termination of this tremor event correlates with any plausible body wave phases.

[24] The second example of abrupt termination of NVT is recorded at ~5900 s, when the longest tremor event during the Sumatra event quits surprisingly fast (Figures 3 and 8). This event continues for ~15 min, and sharply decreases by ~29 times in amplitude in only 30 s to blend into the background noise. As in the previous case, there appears to be no discernible change in the surface wave train during this terminal phase.

5. Discussions and Conclusions

[25] The Mw 9.2 Sumatra earthquake in 2004 triggered an intricate sequence of NVT activity near the SAF in the vicinity of Parkfield. Some NVT is likely triggered by the protracted teleseismic compressional arrivals (*PKP*, *PP*, and *SKP*); these phases generate only tiny normal (~0.15 kPa) and dilatational stresses (~0.8 kPa) beneath the SAF, but are still able to trigger sturdy tremor. *P* waves usually are not considered to have significant triggering potential for the following two reasons. First, it is relatively difficult to separate the high frequency signals caused by the local sources from the signal generated by large events at teleseismic distances. Second, the stress perturbation associated with the *P* wave is usually considered to be too small to cause much dynamic triggering at large distances. Recently, *Fischer et al.* [2008a, 2008b] reported *P* wave-triggered high-frequency bursts in the near field during 1999 Mw 7.6 Chi-Chi, Taiwan, earthquake and the 2004 Mw 6.0 Parkfield earthquake. They estimated a triggering threshold of ~1 kPa. The *P* wave-induced dilatational stress found in this study is comparable to that is found for the high-frequency bursts, although the frequency content of the *P* waves and the triggering distance are quite different. The teleseismic *P* waves of the 2008 Mw 7.9 Wenchuan earthquake also triggered clear tremor near Parkfield [*Peng et al.*, 2009]. Finally, *Miyazawa et al.* [2005] also found remote triggering of the volcanic tremor at Aso volcano in Japan during the *P* waves of the 1999 Mw 7.6 Chi-Chi, Taiwan, earthquake. These observations indicate that tremor source could be sensitive to the small changes in dilatational stress induced by the *P* waves. The duration of excitation may also play a role, and the implausibility of the low normal stresses, which influence Coulomb stress, causing tremor points toward fluid involvement, which is more sensitive to dilatation [e.g., *Miyazawa and Mori*, 2006; *Miyazawa and Brodsky*, 2008].

[26] Clear modulation of NVT activity is evident in the strong bursts of tremor during the passage of large long-period Love waves. Love wave-produced strike-parallel shear stress (~3 kPa) on SAF, although much less than those found in Cascadia and Parkfield triggered by the 2002 Mw 7.8 Denali fault earthquake [*Rubinstein et al.*, 2007; *Peng et al.*, 2008], is close to the threshold from recent surveys of triggered tremor in those regions [*Rubinstein et al.*, 2009; *Peng et al.*, 2009]. In addition, ~400 s period Rayleigh waves also impart stress during this time. In the present geometry, shear stress resolved on a vertical fault from Rayleigh waves is insignificant as Rayleigh waves with strike-parallel incidence generate negligible strike-parallel shear stress on a vertical fault [e.g., *Hill*, 2008]. In contrast, a contribution from dilatational stress to the triggering cannot be readily ruled out. But around 4100 s, soon after the strong bursts of tremor in question, comes the largest amplitude Rayleigh waves. In spite of producing much larger dilatational stress (~4 kPa), we observe relatively reduced NVT action. Hence, we infer that Love wave-induced shear stress is primarily responsible for driving the strongest NVT observed during this teleseism. Moreover, smaller-amplitude tremor bursts during the strongest Rayleigh waves matches better with the short-period oscillation of Love waves (Figure 7), suggesting that even lower-amplitude short-period Love waves are more efficient in exciting the tremor sources than the long-period Rayleigh waves with larger amplitude. These results are consistent with the previous study by *Hill* [2008], which shows that Love waves have a higher triggering potential, compared to Rayleigh waves, when incident on a vertical strike-slip fault. Therefore, shear stress appears to be the most important factor for driving the strongest tremor events in this sequence, which points toward the association of these NVT bursts with shear failure.

[27] Our observations of Love wave triggering of tremor are consistent with other recent studies of triggered tremor in Cascadia [*Rubinstein et al.*, 2009], Parkfield [*Peng et al.*, 2008, 2009] and Taiwan [*Peng and Chao*, 2008]. Recent precise locations of tremor near Cholame, south of Parkfield by *Shelly et al.* [2009] have shown near-linear structures parallel to the SAF strike, suggesting that at least a portion of the tremor occurs on the deep extension of the fault and likely represents shear slip. Finally, studies of tide tremor correlations around Parkfield also found that shear stress fluctuations dominate the triggering process [*Nadeau et al.*, 2008].

[28] On the other hand, *Miyazawa and Mori* [2005] and *Miyazawa and Brodsky* [2008] found that dilatational strain changes and normal stress reduction associated with the passage of Rayleigh waves of the 2003 Tokachi-Oki earthquake and the 2004 Sumatra earthquake are responsible for triggering tremor along the Nankai subduction zone in southwest Japan. *Miyazawa et al.* [2008] suggested that the different observations in Japan and Cascadia (and other places) could be explained by a higher effective friction coefficient and more heterogeneous distribution of fluids in southwest Japan than in other regions. If so, this may result in different behaviors in the observed LFE and NVT signals, and slow slip events at these regions. However, a systematic comparison of the LFE at three subduction zones (southwest Japan, south Vancouver Island, and northern Costa Rica) so far have not found any major difference in the characteristics of the tremor signals [*Brown et al.*, 2009].

[29] In this study we also observed apparently erratic behavior of NVT in some time windows. At times, tremor terminates abruptly without any appreciable change in the character of the teleseismic waves. On the other hand, even after the initial surface waves have subsided, tremor resurges gradually at ~6500 s for ~8 min. These observations suggest that self-moderating tremor. Quick and synchronous changes in amplitude may suggest a localized source of the tremor at that time. A possible explanation can be a sudden change in pore fluid pressure in the system. An abrupt decrease in fluid pressure, for example, would increase the effective normal stress on the fault plane, thereby making slip harder to trigger if shear stress does not increase accordingly.

[30] These findings hint toward some intriguing interpretations. The tremor source is extremely sensitive to very small stress perturbations over a short time scale. Stress changes of as low as ~0.8 kPa probably trigger NVT. Moreover, stress changes sufficient to trigger tremor at one locale may not trigger it shortly before and after, or at other tremor source regions nearby. Decreased tremor action during relatively large stresses implies that tremor generation does not depend only on the magnitude of induced dynamic stress, but other factors also play important roles. These factors may include frequency content and/or duration of the triggering seismic waves, changes in pore fluid pressure, the state of stress on the fault in question, and sometimes involve time delays after the stress is applied.

[31] **Acknowledgments.** The data used in this study come from the High Resolution Seismic Network operated by Berkeley Seismological Laboratory, University of California, Berkeley, the Northern California Seismic Network (NCSN) operated by the U.S. Geological Survey, Menlo Park, and are distributed by the northern California earthquake data center. We thank David Oppenheimer and Doug Neuhauser for extracting the high-sampling rate NCSN data used in this study, and Bob Nadeau for sharing his ambient tremor catalog with us. We thank the Associate Editor, the anonymous reviewer, and Debi Kilb for their constructive remarks and suggestions. The study was supported by the National Science Foundation (grants EAR-0809834, EAR-0809993 and EAR-0711459). Discussions with Joan Gomberg and Emily Brodsky abetted this adventure.

References

Bakun, W. H., et al. (2005), Implications for prediction and hazard assessment from the 2004 Parkfield earthquake, *Nature*, *437*, 969–974, doi:10.1038/nature04067.

Brown, J. R., G. C. Beroza, S. Ide, K. Ohta, D. R. Shelly, S. Y. Schwartz, W. Rabbel, M. Thorwart, and H. Kao, (2009), Deep low-frequency earthquakes in tremor localize to the plate interface in multiple subduction zones, *Geophys. Res. Lett.*, *36*, L19306, doi:10.1029/2009GL040027.

Ellsworth, W. L., J. H. Luetgert, and D. H. Oppenheimer (2005), Borehole array observations of non-volcanic tremor at SAFOD, *Eos Trans. AGU*, *86*(52), Fall Meet. Suppl., Abstract T21A-0443.

Fischer, A. D., Z. Peng, and C. G. Sammis (2008a), Dynamic triggering of high-frequency bursts by strong motions during the 2004 Parkfield earthquake sequence, *Geophys. Res. Lett.*, *35*, L12305, doi:10.1029/2008GL033905.

Fischer, A. D., C. G. Sammis, Y. Chen, and T. Teng (2008b), Dynamic triggering by strong-motion P and S waves: Evidence from the 1999 Chi-Chi, Taiwan, earthquake, *Bull. Seismol. Soc. Am.*, *98*(2), 580–592, doi:10.1785/0120070155.

Ghosh, A., J. E. Vidale, J. R. Sweet, K. C. Creager, and A. G. Wech (2009), Tremor patches in Cascadia revealed by seismic array analysis, *Geophys. Res. Lett.*, *36*, L17316, doi:10.1029/2009GL039080.

Gomberg, J., J. L. Rubinstein, Z. Peng, K. C. Creager, J. E. Vidale, and P. Bodin (2008), Widespread triggering of nonvolcanic tremor in California, *Science*, *319*, 173, doi:10.1126/science.1149164.

Hill, D. P. (2008), Dynamic stresses, Coulomb failure, and remote triggering, *Bull. Seismol. Soc. Am.*, *98*(1), 66–92, doi:10.1785/0120070049.

Ide, S., D. R. Shelly, and G. C. Beroza (2007), Mechanism of deep low frequency earthquakes: Further evidence that deep non-volcanic tremor is generated by shear slip on the plate interface, *Geophys. Res. Lett.*, *34*, L03308, doi:10.1029/2006GL028890.

Ishii, M., P. M. Shearer, H. Houston, and J. E. Vidale (2005), Extent, duration and speed of the 2004 Sumatra–Andaman earthquake imaged by the Hi-Net array, *Nature*, *435*, 933–936, doi:10.1038/nature03675.

Kao, H., S. Shan, H. Dragert, G. Rogers, J. F. Cassidy, and K. Ramachandran (2005), A wide depth distribution of seismic tremors along the northern Cascadia margin, *Nature*, *436*(7052), 841–844, doi:10.1038/nature03903.

Karageorgi, E., R. Clymer, and T. V. McEvilly (1992), Seismological studies at Parkfield. II. Search for temporal variations in wave propagation using vibroseis, *Bull. Seismol. Soc. Am.*, *82*(3), 1388–1415.

Kennett, B. L. N., and E. R. Engdahl (1991), Traveltimes for global earthquake location and phase identification, *Geophys. J. Int.*, *105*, 429–465, doi:10.1111/j.1365-246X.1991.tb06724.x.

Lay, T., and T. C. Wallace (1995), *Modern Global Seismology*, pp. 120–140, Academic, San Diego, Calif.

Lay, T., et al. (2005), The Great Sumatra-Andaman Earthquake of 26 December 2004, *Science*, *308*(5725), 1127–1133, doi:10.1126/science.1112250.

Miyazawa, M., and E. E. Brodsky (2008), Deep low-frequency tremor that correlates with passing surface waves, *J. Geophys. Res.*, *113*, B01307, doi:10.1029/2006JB004890.

Miyazawa, M., and J. Mori (2005), Detection of triggered deep low-frequency events from the 2003 Tokachi-oki earthquake, *Geophys. Res. Lett.*, *32*, L10307, doi:10.1029/2005GL022539.

Miyazawa, M., and J. Mori (2006), Evidence suggesting fluid flow beneath Japan due to periodic seismic triggering from the 2004 Sumatra-Andaman earthquake, *Geophys. Res. Lett.*, *33*, L05303, doi:10.1029/2005GL025087.

Miyazawa, M., I. Nakanishi, Y. Sudo, and T. Ohkura (2005), Dynamic response of frequent tremors at Aso volcano to teleseismic waves from the 1999 Chi-Chi, Taiwan earthquake, *J. Volcanol. Geotherm. Res.*, *147*, 173–186, doi:10.1016/j.jvolgeores.2005.03.012.

Miyazawa, M., E. E. Brodsky, and J. Mori (2008), Learning from dynamic triggering of low-frequency tremor in subduction zones, *Earth Planets Space*, *60*(10), e17–e20.

Nadeau, R. M., and D. Dolenc (2005), Nonvolcanic tremors deep beneath the San Andreas fault, *Science*, *307*, 389, doi:10.1126/science.1107142.

Nadeau, R. M., A. M. Thomas, and R. Burgmann (2008), Tremor-tide correlations at Parkfield, CA, *Eos Trans. AGU*, *89*(53), Fall Meet. Suppl., Abstract U33A-0053.

Nakata, R., N. Suda, and H. Tsuruoka (2008), Non-volcanic tremor resulting from the combined effect of Earth tides and slow slip events, *Nat. Geosci.*, *1*, 676–678, doi:10.1038/ngeo288.

Obara, K. (2002), Nonvolcanic deep tremor associated with subduction in southwest Japan, *Science*, *296*, 1679–1681, doi:10.1126/science.1070378.

Oppenheimer, D., F. Klein, J. Eaton, and F. Lester (1993), The northern California seismic network bulletin January–December 1992, *U.S. Geol. Surv. Open File Rep.*, *93-578*.

Payero, J. S., V. Kostoglodov, N. Shapiro, T. Mikumo, A. Iglesias, X. Pérez-Campos, and R. W. Clayton (2008), Nonvolcanic tremor observed in the Mexican subduction zone, *Geophys. Res. Lett.*, *35*, L07305, doi:10.1029/2007GL032877.

Peng, Z., and K. Chao (2008), Non-volcanic tremor beneath the Central Range in Taiwan triggered by the 2001 Mw 7.8 Kunlun earthquake, *Geophys. J. Int.*, *175*(2), 825–829, doi:10.1111/j.1365-246X.2008.03886.x.

Peng, Z., J. E. Vidale, K. C. Creager, J. L. Rubinstein, J. Gomberg, and P. Bodin (2008), Strong tremor near Parkfield, CA, excited by the 2002 Denali fault earthquake, *Geophys. Res. Lett.*, *35*, L23305, doi:10.1029/2008GL036080.

Peng, Z., J. E. Vidale, A. Wech, R. M. Nadeau, and K. C. Creager (2009), Remote triggering of tremor along the San Andreas fault in central California, *J. Geophys. Res.*, *114*, B00A06, doi:10.1029/2008JB006049.

Peterson, C. L., and D. H. Christensen (2009), Possible relationship between nonvolcanic tremor and the 1998–2001 slow slip event, south central Alaska, *J. Geophys. Res.*, *114*, B06302, doi:10.1029/2008JB006096.

Rogers, G., and H. Dragert (2003), Episodic tremor and slip on the Cascadia subduction zone: The chatter of silent slip, *Science*, *300*, 1942–1943, doi:10.1126/science.1084783.

Rubinstein, J. L., J. E. Vidale, J. Gomberg, P. Boudin, K. C. Creager, and S. D. Malone (2007), Non-volcanic tremor driven by large transient shear stresses, *Nature*, *448*, 579–582, doi:10.1038/nature06017.

Rubinstein, J. L., M. L. Rocca, J. E. Vidale, K. C. Creager, and A. G. Wech (2008), Tidal modulation of nonvolcanic tremor, *Science*, *319*, 186–189, doi:10.1126/science.1150558.

Rubinstein, J. L., J. Gomberg, J. E. Vidale, A. G. Wech, H. Kao, K. C. Creager, and G. Rogers (2009), Seismic wave triggering of nonvolcanic tremor, episodic tremor and slip, and earthquakes on Vancouver Island, *J. Geophys. Res.*, *114*, B00A01, doi:10.1029/2008JB005875.

Schwartz, S. Y., and J. M. Rokosky (2007), Slow slip events and seismic tremor at circum-Pacific subduction zones, *Rev. Geophys.*, *45*, RG3004, doi:10.1029/2006RG000208.

Shelly, D. R., G. C. Beroza, S. Ide, and S. Nakamula (2006), Low-frequency earthquakes in Shihoku, Japan, and their relationship to episodic tremor and slip, *Nature*, *442*, 188–191, doi:10.1038/nature04931.

Shelly, D. R., G. C. Beroza, and S. Ide (2007a), Non-volcanic tremor and low-frequency earthquake swarms, *Nature*, *446*(7133), 305–307, doi:10.1038/nature05666.

Shelly, D. R., G. C. Beroza, and S. Ide (2007b), Complex evolution of transient slip derived from precise tremor locations in western Shikoku, Japan, *Geochem. Geophys. Geosyst.*, *8*, Q10014, doi:10.1029/2007GC001640.

Shelly, D. R., W. L. Ellsworth, T. Ryberg, C. Haberland, G. S. Fuis, J. Murphy, R. M. Nadeau, and R. Bürgmann (2009), Precise location of San Andreas fault tremors near Cholame, California using seismometer clusters: Slip on the deep extension of the fault?, *Geophys. Res. Lett.*, *36*, L01303, doi:10.1029/2008GL036367.

Taira, T., P. G. Silver, F. Niu, and R. M. Nadeau (2009), Remote triggering of fault-strength changes on the San Andreas fault at Parkfield, *Nature*, *461*, 636–639, doi:10.1038/nature08395.

Thorwart, M., W. Rabbel, and W. Taylor (2007), Non-volcanic tremors in Costa Rica, *Eos Trans. AGU*, *88*(52), Fall Meet. Suppl., Abstract T21A-0351.

Thurber, C., H. Zhang, F. Waldhauser, J. Hardebeck, A. Michael, and D. Eberhart-Phillips (2006), Three-dimensional compressional wavespeed model, earthquake relocations, and focal mechanisms for the Parkfield, California, region, *Bull. Seismol. Soc. Am.*, *96*(4B), S38–S49, doi:10.1785/0120050825.

Wech, A. G., and K. C. Creager (2008), Automated detection and location of Cascadia tremor, *Geophys. Res. Lett.*, *35*, L20302, doi:10.1029/2008GL035458.

West, M., J. J. Sánchez, and S. R. McNutt (2005), Periodically triggered seismicity at Mount Wrangell, Alaska, after the Sumatra earthquake, *Science*, *308*, 1144–1146, doi:10.1126/science.1112462.

K. C. Creager, A. Ghosh, H. Houston, and J. E. Vidale, Department of Earth and Space Sciences, University of Washington, Johnson Hall, Room 70, Box 351310, Seattle, WA 98195-1310, USA. (aghosh.earth@gmail.com)

Z. Peng, School of Earth and Atmospheric Sciences, Georgia Institute of Technology, 311 Ferst Dr., Atlanta, GA 30332-0340, USA.